INL/CON-14-33459
PREPRINT

Microstructural Characterization of Alloy 617 Crept into the Tertiary Regime

2015 ASME Pressure Vessels & Piping Conference

Thomas M. Lillo and Richard N. Wright

July 2015

The INL is a
U.S. Department of Energy
National Laboratory
operated by
Battelle Energy Alliance

Proceedings of the 2015 ASME Pressure Vessels & Piping Conference
PVP ASME 2015
July 19-23, 2015, Boston, Massachusetts, USA

PVP2015-45055

Microstructural Characterization of Alloy 617 Crept into the Tertiary Regime

Thomas M. Lillo
Idaho National Laboratory
Idaho Falls, Idaho, USA

Richard N. Wright
Idaho National Laboratory
Idaho Falls, Idaho, USA

ABSTRACT

The dislocation structure and area fraction of creep voids in Alloy 617 were characterized following creep tests interrupted at total creep strains ranging from 2-20%. A range of creep temperatures (750-1000°C) and initial creep stresses (10-145 MPa) produced creep test durations ranging from 1 to 5800 hours. Image analysis of optical photomicrographs on longitudinal sections of the gage length was used to document the fraction of creep porosity as a function of creep parameters. In interrupted creep tests performed at 750°C, minimal levels of creep porosity were found even in samples crept to ~20% total creep strain. At 1000°C, creep porosity was negligible below total creep strains of 10% and increased thereafter with increasing total creep strain. Also, creep porosity increased with decreasing creep stress for a given total creep strain. TEM performed on the gage sections did not reveal significant creep void formation on grain boundaries or in the grains at the sub-micron level. However, dislocation boundaries exhibited extensive dislocation rearrangement and dislocation-dislocation reactions. It was concluded that the onset of tertiary creep did not result from creep void formation and more likely arose due to the formation of low energy dislocation substructures.

NOMENCLATURE

$\dot{\varepsilon}_{min}$	Minimum creep rate
D	Diffusion coefficient of the matrix
σ	Applied stress
μ	Shear modulus
b	Burgers vector
k	Boltzman constant
T	Temperature
n	Stress exponent
f	Void fraction
σ	Applied stress
t	Time
$\dot{\varepsilon}_o$	Temperature-dependent constant
σ_{ref}	Reference stress (generally either Young's modulus or the shear modulus)

INTRODUCTION

The maximum use temperature of 1000°C for Alloy 617 in a proposed Very High Temperature Reactor (VHTR) heat exchanger is a significant design consideration because significant atomic mobility and creep deformation can be expected to occur even at very low applied stresses. From an engineering perspective, the creep mechanism most likely to be operational is dislocation climb/glide resulting in power law creep behavior. (Purely diffusional creep processes – Nabarro-Herring creep, Coble creep, etc. – result in creep rates so low as to be insignificant over component lifetime but require a large wall thickness that is not economically viable.) Creep curves of many engineering materials exhibit three distinct regimes – primary creep, secondary creep and tertiary creep. In many material systems, primary and secondary creep represent the majority of the creep life of the material while tertiary is relatively short. However, previous work with Alloy 617 has suggested a relatively short primary and secondary creep regime followed by a lengthy tertiary creep regime prior to rupture.

The three stages of classical creep curves are considered to be the result of microstructural changes. Primary creep involves the generation, glide and entanglement of lattice dislocations resulting in hardening. Secondary creep is thought to represent the balance between hardening mechanisms and recovery mechanisms. Finally, failure occurs in the tertiary creep regime with the growth and linkup of voids. The onset of tertiary creep, i.e. the transition from secondary to tertiary creep behavior, is poorly understood, even though this is an important criterion for design of high temperature nuclear components. Although creep void growth and linkup are responsible for rupture it is not clear whether they are the root cause of the transition to tertiary creep through loss of cross sectional area, increasing in the effective creep stress and thus the creep rate, or simply a secondary – and perhaps, unrelated or weakly coupled– phenomenon with an alternate mechanism dominant in the onset of tertiary behavior.

The study reported here was undertaken to characterize creep void formation and dislocation substructures in Alloy 617 crept at high temperatures to ascertain their role in the transition to tertiary creep behavior. Understanding of the transition from secondary to tertiary creep behavior will aid in setting the limits of tertiary creep deformation for engineering purposes and, potentially, suggest developmental strategies aimed at delaying the onset of tertiary creep, thus increasing the useful creep life of high temperature, structural alloys.

Table 1. Composition of Alloy 617 Plate

Element	C	Cr	Ni	Mn	Si	Mo	Ti	Cu	Fe	Al	Co
Conc., wt%	0.05	22.2	54.1	0.1	0.1	8.6	0.4	0.04	1.6	1.1	11.6

Note: Boron <0.001 wt% and sulfur <0.002 wt%.

EXPERIMENTAL

Creep specimens with a nominal diameter of 6.35 mm and an adjusted gage length of 34.5 mm were fabricated from rolled and solution treated, thick plate (nominally 38.1 mm x 1397 mm x 3505.2 mm) of Alloy 617 (VDM Heat Number 314626), see Table 1 for the vendor-supplied Certificate of Analysis of the composition. Creep tests were performed in accordance with ASTM Standard E 139-06, with extensometer attachment outside the reduced section of the specimens. The displacement from two linear displacement transducers on the extensometer was recorded as a function of time. Creep curves were generated from the average of two displacement transducers. Temperature was controlled and monitored to within ±2.5°C with two Type R thermocouples secured to the gage section of the sample using platinum wire according to ASTM Standard E 633-00. The majority of the creep tests were run at two temperatures, 750 and 1000°C, and at two stress levels at each temperature. Interrupted creep tests were run to a total creep strain of approximately 2%, 5%, 10% and 20% at both temperatures for metallurgical evaluation. Additional creep tests were run to a creep strain of 20% at 1000°C under various creep stresses to provide additional insight into the effect of initial creep stress on creep behavior and creep void fraction. A few creep tests were also run to a total creep strain of 20% at 800 and 900°C to gain a better understanding of the effect of temperature on the resulting creep void area fraction. Also a number of creep tests were run to rupture to obtain the full creep curve, the time to rupture, the time to reach 20% creep strain and the time to the transition to tertiary creep behavior.

The gage section of each specimen from each interrupted creep test, containing the minimum gage diameter, was prepared for optical metallography and mounted to produce a longitudinal section along the gage length. After mechanical polishing down to 3 micron alumina, the entire polished gage section was electropolished (Struers LectroPol-5) in a solution of ethanol-10% water-10% ethylene glycol monobutyl ether-7% perchloric acid to remove flowed metal from the creep voids that may have occurred during mechanical polishing. Metallography samples were then subjected to vibratory polishing using 0.05 micron colloidal silica for 1 hour. Automated image acquisition (Zeiss Axio Observer.Z1M) of the entire gage section was carried out at 200x The area of each individual photograph was approximately 0.4 mm^2 while the total area of the gage section analyzed was on the order of 80 mm^2 (approximately 200 photographs covering the gage length). The possibility existed that the porosity was not homogeneously distributed throughout the gage section, especially at the higher interrupted strains, so following this initial porosity analysis approximately 200-500 microns of material were removed from the metallography mounts and the porosity analysis repeated. The porosity analysis was repeated a third time after removal of an additional 200-500 microns of material. Approximately 240 mm^2 of area was analyzed through the gage section of each sample. Each photograph from the three sections was individually analyzed for porosity using image analysis (AxioVision 4, version 4.8.2.0) and reported as a percentage of the image area. The average porosity in the gage section was calculated by averaging the area fraction of porosity in all photographs.

Part of the reduced gage section was reserved for making TEM samples to look for creep cavitation at length scales below the resolution of optical metallography and to characterize the dislocation structure. TEM samples were made with orientations parallel (longitudinal) and perpendicular (transverse) to the stress axis of the creep sample.

Results

Microstructure – Figure 1 shows the as-received microstructure of the solution annealed plate. The grain size is quite large (>100 μm) as a result of the high temperature, solution anneal. There is evidence of a bi-modal grain size distribution, though not as prominent as reported previously for Alloy 617 produced by a different vendor [1]. Recrystallization twins are also evident in the microstructure of Fig. 1. Carbides and nitrides appear as the gray particles.

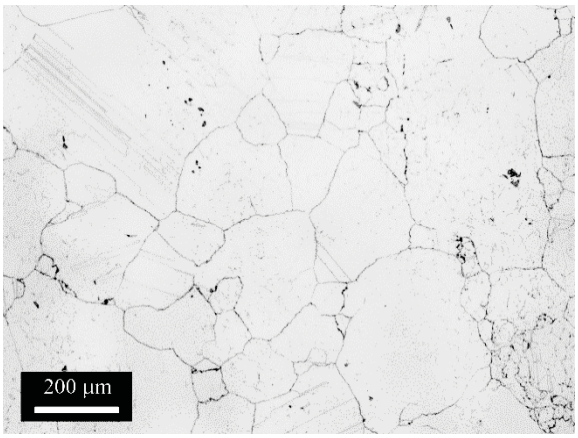

FIG 1. AS-RECEIVED ALLOY 617 MICROSTRUCTURE.

Figure 2 shows the as-polished (unetched) microstructure for creep tests run at 1000°C and an initial creep stress of either 16 MPa or 20 MPa. The micrographs in Fig. 2, contain the area of maximum porosity fraction in the gage section, as

determined by image analysis, for each creep test at the creep strain indicated beneath each photograph. The area fraction of creep porosity increases with creep strain although porosity fractions are still quite small in all cases. No porosity formation is observed at the optical level of resolution at a creep strain of 5% or below at 20 MPa (Figs. 2e and 2f). In general, porosity formation appears to be more extensive in the creep tests run at 16 MPa compared to those run at 20 MPa. This is most easily seen by comparing the micrographs in Figs. 2d and 2h, corresponding to creep tests carried out at 1000°C to a total creep strain of 20% with an initial creep stress of 16 and 20 MPa, respectively.

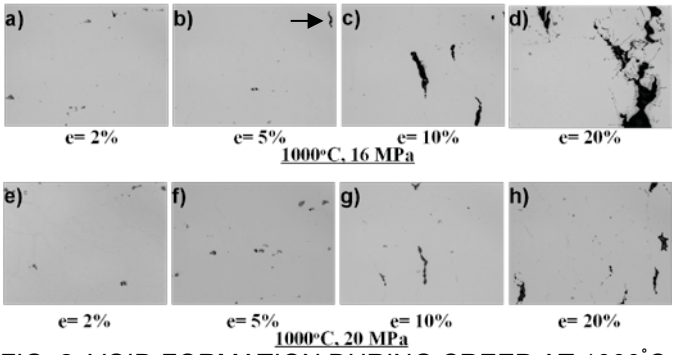

FIG. 2. VOID FORMATION DURING CREEP AT 1000˚C

Analysis of creep porosity: The average porosity, as a percentage of the total area analyzed in the gage section, is plotted in Fig. 3a & b, for 750°C and 1000°C, respectively, as a function of the interrupted creep strain. (Standard error is used in this and subsequent figures to generate the error bars.) At 750°C, creep porosity fractions are very small - even at very high total creep strains of 20%. Also, the porosity fraction that develops at 750ºC for a given interrupted strain does not appear to be strongly dependent on the initial creep stress. At 1000°C, creep porosity is not evident below approximately 5% creep strain and only becomes significant when the total creep strain exceeds about 10%, with the exception of the creep test run at 1000°C and 10 MPa in Fig. 3b. Above a total creep strain of 5%, the porosity fraction steadily increases as the creep strain increases.

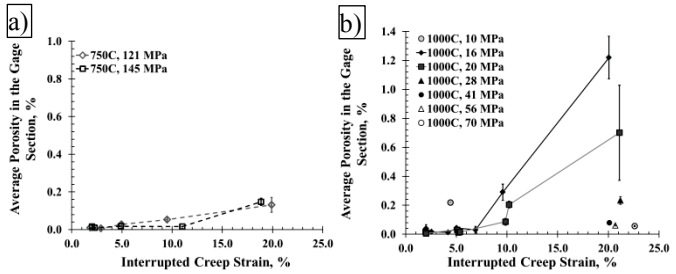

FIG. 3. CREEP POROSITY VS. INTERRUPTED CREEP STRAIN AT A) 750°C AND B) 1000°C

Also, at 1000°C, higher levels of porosity develop at lower values of the initial creep stress for a given total creep strain, Fig. 3b. This is especially evident for an interrupted creep strain of 20% where relatively little creep porosity is found in samples tested at high initial creep stress values of 56 and 70 MPa compared to samples tested at 16 and 20 MPa. Decreasing initial creep stress results in a non-linear increase in the time required to attain a given creep strain, Fig. 4, due to the power law relationship for creep, with the minimum creep rate defined by Eqn. 1[2-4], in the stress range used in this study.

$$\dot{\varepsilon}_{\min} \propto D\frac{\mu b}{kT}\left(\frac{\sigma}{\mu}\right)^{n} \qquad [1]$$

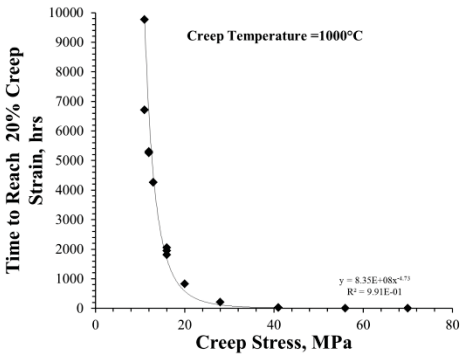

FIG. 4. INFLUENCE OF APPLIED CREEP STRESS ON CREEP TIME.

The stress exponent, n, for this heat of Alloy 617 has been shown to be approximately 5.6 [5], indicating the minimum strain rate is quite sensitive to the initial stress, and thus, the time to reach a given strain is expected to be quite sensitive to the initial stress. Significantly more time is available for creep void growth when achieving a given total creep strain at lower creep stresses and results in increased porosity fractions. Figure 5 more explicitly shows this dependence of the average porosity fraction on the initial creep stress at a constant creep strain of 20%. This dependency appears to be very similar to that of the time dependency of the initial creep stress to reach 20% creep strain, shown in Fig. 4.

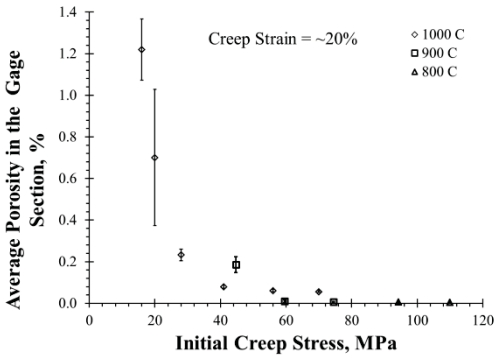

FIG. 5. EFFECT OF INITIAL CREEP STRESS ON CREEP POROSITY

Transition to tertiary behavior –Creep cavitation effectively reduces the cross sectional area of the gage section and results in increasing stress in the gage area. If the creep void fraction becomes large enough accelerated creep may occur and

produce the transition from secondary, or minimum creep, behavior to tertiary creep in constant load creep tests. The average creep porosity as a function of the tertiary creep strain (total creep strain minus the strain attributed to primary and secondary creep), has been plotted in Fig. 6a while the average creep porosity as a function of the time spent in the tertiary creep regime has been plotted in Fig. 6b for tests run at 1000°C. Porosity is negligible at the beginning of the tertiary creep regime and increases with increasing tertiary creep strain and the time spent in the tertiary creep regime. The fractions of porosity at the start of the tertiary regime are too low to significantly affect the stress in the gage section, thus, the accelerated creep rate in this region is likely caused by another mechanism.

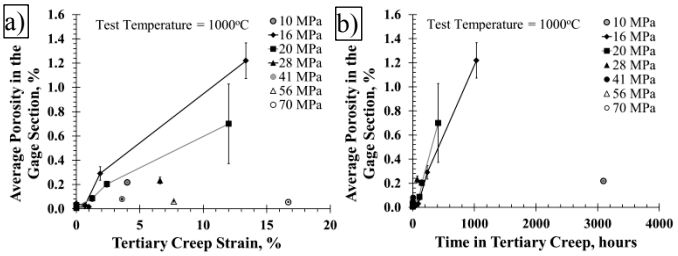

FIG. 6. EFFECT OF TERTIARY CREEP STRAIN AND TIME ON CREEP POROSITY.

Whereas the creep tests run at 750°C show a fairly consistent creep strain at the transition to tertiary behavior, around 0.2-0.7, the creep strain at the transition to tertiary creep behavior at 1000°C shows considerable variation with the initial stress. Figure 7 shows the relationship between initial creep stress and the creep strain at which the creep behavior transitions to tertiary-type behavior. This plot shows a fairly large maximum (total creep strain = ~16.5%) at intermediate initial creep stresses with low values at both low and high stresses. Figure 7 suggests intermediate creep stresses delay the transition to tertiary creep behavior as compared to either low or high initial creep stresses. Therefore, at 1000°C for a given *total* creep strain, the amount of strain in the tertiary regime is a function of the initial creep stress. This behavior was not observed in specimens crept at 750°C for the conditions examined here. It may have been observed if creep tests were run at significantly lower initial stresses; unfortunately, such tests would require a very long time to complete due to the very low creep rates dictated by the power law creep behavior.

TEM observations around the transition to tertiary behavior: The average porosity fraction measured in the optical micrographs was quite small with the highest average porosity value being less than 1.5% for an interrupted creep strain of 20% (1000°C and 16 MPa); well after the transition to tertiary creep behavior. Therefore, it seems unlikely that a reduction in the effective cross section of the creep sample due creep porosity could be responsible for the rapidly increasing creep rate characteristic of the tertiary creep regime. Therefore,

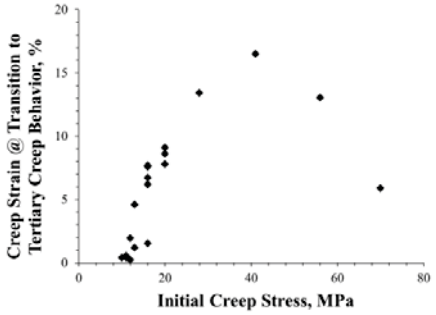

FIG. 7. EFFECT OF CREEP STRESS ON TERTIARY TRANSITION STRAIN.

transmission electron microscopy (TEM) was used to search for significant amounts of porosity on a scale below the resolution of optical microscopy and/or search for other explanations for the rapidly increasing creep rate in the tertiary regime exhibited by Alloy 617. At least 10 samples from the gage section of selected interrupted creep samples were examined using TEM.

0% Tertiary Creep Strain – Generally, samples crept to 2% and 5% total creep strain at creep stresses of either 16 or 20 MPa at 1000°C did not exhibit a transition to tertiary creep in their associated creep curves, with the exception of one sample tested at16 MPa, 1000°C and a total creep strain of 2.5%.

2% Total Creep Strain (0% tertiary creep strain) @ 1000°C: Figure 8 shows representative bright field micrographs of the microstructures found in the gage section of creep samples crept at 1000°C to a total of 2% total creep strain at initial creep stress values of 16 and 20 MPa. As mentioned above, these samples exhibited only primary and secondary creep behavior and did not experience a transition to tertiary creep (tertiary creep strain ~0%). Generally, the microstructures show a relatively low density of individual dislocations randomly distributed throughout the grains or present in slip bands, e.g. Fig. 8h. However, Fig. 8f does seem to show the beginnings of organized dislocation substructures but generally no highly organized dislocation substructures are present. No evidence of fine porosity on grain boundaries, in the vicinity of grain boundary carbides or associated with intragranular precipitates could be found in any of these creep samples.

5% Total Creep Strain (0% tertiary creep strain) at 1000°C: Samples crept to a total of 5% creep strain at 16 MPa and 20 MPa tend to show a somewhat higher dislocation density and the beginnings of dislocation cell walls, Fig. 9, although they appear to be more accurately described as dense tangles of lattice dislocations. The creep curves associated with these samples, again, did not show evidence of a transition to tertiary creep, i.e. tertiary creep ~0%. Evidence also was lacking of significant amounts of porosity on a fine scale in these samples. However, the features at the arrows in Fig. 9b may be small pores, although, they may also be fine carbide precipitates or pitting due to electropolishing. This was the only location in any of the samples crept to 5% creep strain that exhibited features that could possibly be attributed to creep cavitation, thus, incidences of creep cavitation at the sub-micron scale are deemed to be rare and insignificant in affecting creep behavior.

FIG. 8. MICROSTRUCTURE IN THELONGITUDINAL AND TRANSVERSE DIRECTIONS OF SAMPLES CREPT TO ~2% STRAIN (0% TERTIARY STRAIN) AT 16 AND 20 MPA.

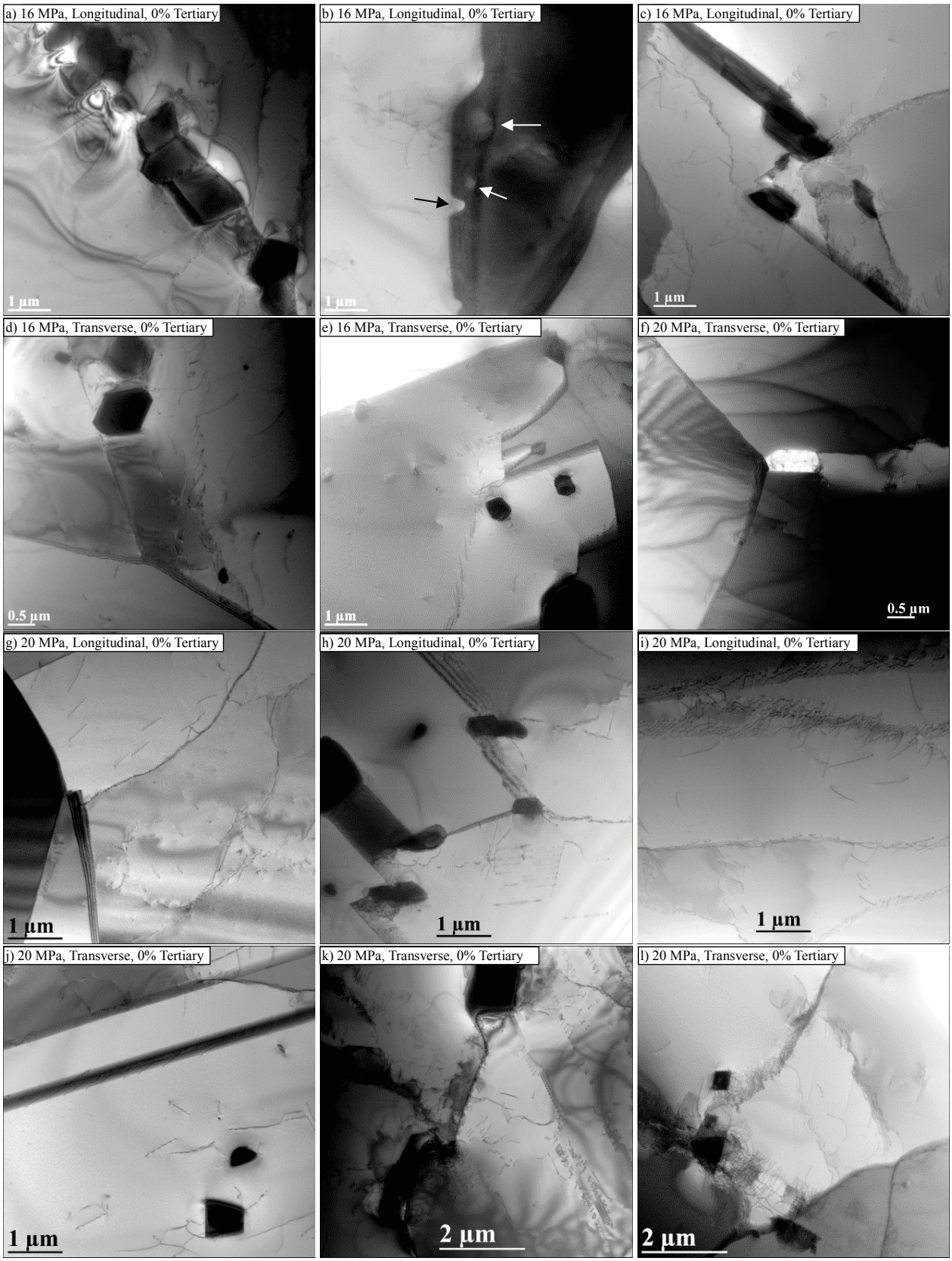

Fig. 9. MICROSTRUCTURE IN THELONGITUDINAL AND TRANSVERSE DIRECTIONS OF SAMPLES CREPT TO ~5% STRAIN (0% TERTIARY STRAIN) AT 16 AND 20 MPA.

Non-zero Tertiary Creep – In samples crept to total creep strains in excess of 5%, tertiary creep behavior was evident in the creep curves and was present to different extents in these samples due to the influence of the initial creep stress on the creep strain at the transition to tertiary behavior, illustrated in Fig. 7.

0.7% Tertiary Creep Strain at 16 MPa and 1000°C : Figure 10 a-c indicate the dislocation substructure to be more organized than in samples without any tertiary creep strain and the grain interior is relatively free of individual dislocations (compare with Figs. 8 & 9). Figure 10c shows a grain boundary precipitate as a source of dislocations, most likely due to strains associated with thermal expansion mismatch between the precipitate and the matrix. No evidence of creep cavitation on a microscopic level was detected in these samples (total creep strain ~7%).

1.3% Tertiary Creep Strain at 20 MPa and 1000°C: Figure 10d-f show the microstructure associated with approximately twice the level of tertiary creep strain as that shown in Figs 10a-c. The dislocation density is elevated with dislocation slip bands evident in Figs. 10d and 10f. The dislocations in the sub-grains are more organized with evidence of dislocation-dislocation reactions to form lower energy boundaries, see arrow at bottom left corner of Fig. 10f.

2.4% Tertiary Creep Strain at 20 MPa and 1000°C: Figure 10g-i show microstructures representative of almost twice as

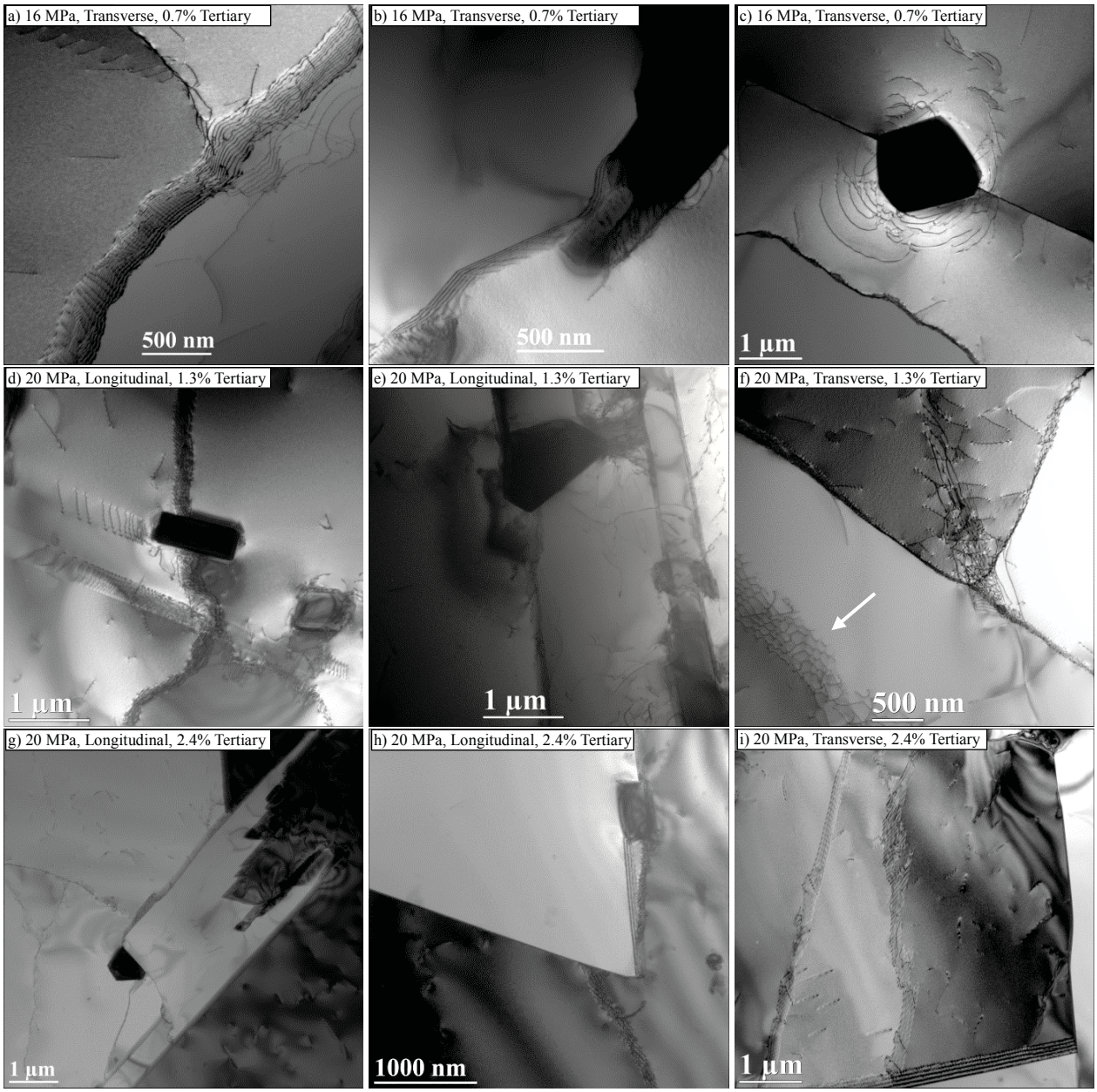

FIG. 10. MICROSTRUCTURE OF SPECIMENS CREPT TO 0.7, 1.3 AND 2.4% IN THE TERTIARY CREEP REGIME AT 16 AND 20 MPA.

much tertiary creep strain as those of Figs. 10d-f (and almost 4x that of Figs. 10a-c). The differences compared to Fig. 10d-f are relatively minor. Grain interiors are relatively free of lattice dislocations. Dislocation slip bands are not as prevalent but the dislocation cell walls are more developed. No creep cavitation was observed in any of these samples.

DISCUSSION

The results presented above focus mainly on creep tests that were preformed above 750°C. The main reason for this is that gamma prime particles (nominally, Ni_3Al) precipitate at this temperature and impart significant strengthening to this alloy during creep testing [5]. As these particles grew in size during the creep test, their influence on creep behavior is reduced. Due to this complication, the creep behavior of the samples tested at 750°C was not analyzed in detail. However, Fig. 3a shows minimal creep cavitation even in creep tests interrupted at 20% total creep strain. This suggests that the presence of fine gamma prime particles does not result in increased creep cavitation and there is reason to believe that the points to be made below concerning the results of the 1000°C creep tests are valid for this lower test temperature.

Root Cause of the Transition to Tertiary Creep Behavior – The main conclusion that can be drawn from the information presented here is that the transition to tertiary creep ***is not*** due to creep cavitation and the associated reduction of the effective cross sectional area of the gage diameter. Significant amounts of creep cavitation on a microscopic level were not found during TEM examinations, even on creep samples subjected to more than ~10% total creep strain (and tertiary creep strain in excess of 2%).Therefore, the creep cavitation measured in optical micrographs includes virtually all the creep porosity that developed in the sample during creep testing. The reduction in the effective cross sectional area due to creep porosity at the transition to tertiary creep behavior is small (<1%) and unlikely to result in the rapidly increasing creep rate exhibited in the tertiary creep regime of this alloy. The transition to tertiary creep is more likely due to another mechanism or mechanisms. Evidence in support of the formation of low energy dislocation substructures, LEDS, was observed. LEDS are thought to be responsible for the transition to tertiary behavior by a growing number of researchers [6-10]. Figure 11 show instances of the formation of highly geometric dislocation structures within cell walls. These geometric structures can only be made by rearrangement and interaction of dislocations within the cell wall to form low energy dislocation structures. These low energy dislocation networks effectively reduce the dislocation density, increase the mean-free path of mobile dislocations during creep as well as reduce the long range stresses arising from dislocation cell walls that would arise from less organized dislocation networks.

Figure 7 shows that the magnitude of the initial creep stress may be influencing the development of low energy dislocation (LED) structures. Although TEM was not performed on samples subjected to intermediate creep stresses,

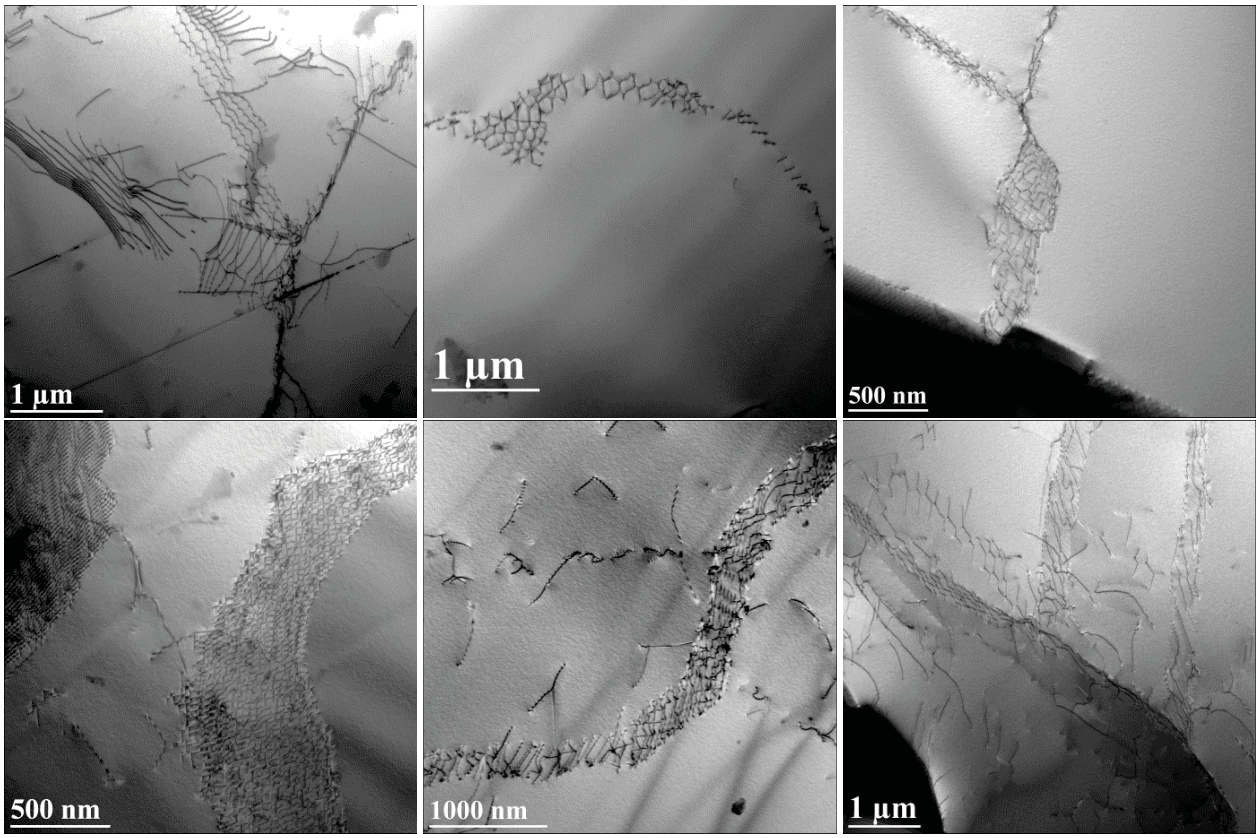

FIG. 11. EXAMPLES OF LOW ENERGY DISLOCATION STRUCTURES FORMED IN THE TERTIARY CREEP REGIME.

one can postulate that these LED structures develop quickly at both very low creep stresses as well as at very high creep stresses, although most likely for different reasons. At low creep stresses the dislocation velocity is sufficiently low to allow time for rearrangement of the dislocations into LED structures. At high creep stresses there is a high density of dislocation tangles and a high driving force (large reduction in energy) to arrange into LED structures. At intermediate creep stress levels, the combination of more rapidly moving dislocations without a high driving force to rearrange acts to suppress the development of LED structures. However, additional creep tests using intermediate creep stresses that are interrupted around the transition to tertiary behavior followed by TEM analysis of the microstructure is needed to verify this hypothesis.

Porosity Development – Void growth due to atom fluxes from voids to grain boundaries is well documented and analyzed [11-13]. Cocks, et. al [11] have generally shown creep void growth results from material diffusing out of the void to the grain boundary, limited by either grain boundary diffusion or surface diffusion along the void surface, or due to power law creep. The relationships they derive for the rate of void growth are dependent on the applied stress as:

Grain Boundary Diffusion limited: $\frac{df}{dt} \propto \sigma$

Surface Diffusion limited: $\frac{df}{dt} \propto \sigma^3$

Power Law Creep dominated: $\frac{df}{dt} \propto \sigma^n$

Furthermore, they show that the diffusional processes, grain boundary diffusion-limited or surface diffusion-limited, are dominant at low void fractions (generally <1%) and then transitions to the power law creep mechanism at higher void fractions. Since this study reveals relatively low void fractions, generally <1%, it is likely void growth is being dominated by a diffusional process throughout most of the interrupted creep tests. While void growth is occurring, the alloy is deforming by power law creep in the range of creep stresses in this study [5] according to:

$$\dot{\varepsilon}_{min} = \dot{\varepsilon}_o \left(\frac{\sigma}{\sigma_{ref}}\right)^{5.6} \qquad [2]$$

Therefore, if the two processes can be thought of as independent, which is reasonable at low void fractions [11], then a small increase in stress will significantly increase the minimum creep rate, with a stress exponent of ~5.6, relative to the void growth rate, with a stress exponent of only 1 or 3. Thus, as the creep stress increases the creep rate increases rapidly but the rate of creep void growth increases to a much lesser degree due to its smaller stress exponent. The net result is that time to achieve a given creep strain decreases drastically and there is relatively less time for voids to grow. Therefore, creep tests run to a given creep strain at higher creep stresses develop a lower fraction of porosity than those tests run at a low creep stress, as show in Fig. 3b and Fig. 5. So porosity will be more of an issue at low values of creep stress. However, it will take much longer to achieve a limiting creep strain. So it remains to be determined whether creep void growth will be an issue during the lifetime of a high temperature component when its design life is determined by a limiting tertiary creep strain.

CONCLUSIONS

This study on the microstructure and creep void fractions in interrupted creep tests of Alloy 617 at temperatures of 750-1000°C has revealed the following:

- The average creep void fraction is very small (≤0.1%) in specimens tested at 750°C and total creep strains up to about 20%.
- At 1000°C:
  - Creep porosity is negligible at total creep strains of ≤ 5%
  - Creep porosity fraction increases as creep strain increases above a creep strain of 5% but still remain relatively low (~1%) even at total creep strains of up to 20%
  - Creep porosity fractions increase as the initial creep stress decreases for tests carried out to the same interrupt creep strain. This suggests lower initial creep stresses allow relatively more time for creep void growth for a given interrupted creep strain
- Minimal creep porosity was observed at the onset of tertiary creep behavior, suggesting creep void growth is not responsible for the transition to tertiary creep behavior
- TEM analysis of crept microstructures shows the development of low energy dislocation (LED) structures near the onset of tertiary creep behavior and are likely responsible for the transition in creep behavior.

REFERENCES

1. T. Lillo, J. Cole, M. Frary, S. Schegel, "Influence of Grain Boundary Character on Creep Void Formation in Alloy 617", Met. And Matls. Trans. A, vol. 40A, 2009, pp. 2803-2811.
2. R.S.W. Shewfelt and L.M. Brown, "High-temperature strength of dispersion-hardened single crystals II. Theory", Philos. Mag., 1977, vol. 35, pp. 945-962.
3. R. Lagneborg, "Bypassing of dislocations past particles by a climb mechanism", Scr. Metall., 1973, vol. 7, pp. 605-613.
4. H.E. Evans and G. Knowles, "Threshold stress for creep on dispersion-strengthened alloys", Met. Sci., 1980, vol. 14, pp. 262-266.

5. J.K. Benz, L.J. Carroll, J.K. Wright, R.N. Wright and T.M. Lillo, “Threshold Stress Creep Behavior of Alloy 617 at Intermediate Temperatures”, Met. And Matls. Trans. A, 2014, DOI 10.1007/s11661-014-2244-y
6. D. Kuhlmann-Wilsdorf, “Theory of Plastic Deformation: - properties of low energy dislocation structures”, Matls. Sci. Eng., vol. A113, 1989, pp. 1-41.
7. A.K. Mukherjee, J.E. Bird and J.E Dorn, “Experimental Correlations for High Temperature Creep”, Trans. of the ASM, vol. 62, 1969, pp. 155-179.
8. S. Takeuchi and A.S Argon, “Review: Steady-state creep of single-phase crystalline matter at high temperature”, J. Matls. Sci., vol. 11, 1976, pp. 1542-1566.
9. M.C. Carroll and L.J. Carroll, “Developing Dislocation Subgrain Structures and Cyclic Softening During High-Temperature Creep-Fatigue of a Nickel Alloy”, Met. And Matls. Trans. A, vol. 44A, 2013, pp. 3592-3607.
10. J.L. Martin, A.S. Argon, “Low Energy Dislocation Structures due to Recovery and Creep”, Mat. Sci. and Engg., vol. 81, 1986, pp. 337-348.
11. A.C.F. Cocks, M.F. Ashby, “On Creep Fracture by Void Growth”, Prog. Matls. Sci., vol. 27, 1982, pp. 189-244.
12. D.S. Wilkinson, “A Model for Creep Cracking by Diffusion-controlled Void Growth”, Mat. Sci and Engg., vol. 49, 1981, pp. 31-39.
13. S. Traiviratana, E.M. Bringa, D.J. Benson, M.A. Meyers, “Void growth in metals: Atomistic calculations”, Acta Mater., vol. 56, 2008, pp. 3874-3886.